Scanning Microscopy

Volume 6 | Number 2 Article 4

3-24-1992

Visualizing Cells in Three Dimensions Using Confocal Microscopy, Image Reconstruction and Isosurface Rendering: Application to Glial Cells in Mouse Central Nervous System

Frank Morgan
University of Connecticut

Elisa Barbarese
University of Connecticut

John H. Carson
University of Connecticut

Scanning Microscopy, Vol. 6, No. 2, 1992 (Pages 345-357)
Scanning Microscopy International, Chicago (AMF O'Hare), IL 60666 USA

0891-7035/92$5.00+.00

VISUALIZING CELLS IN THREE DIMENSIONS USING CONFOCAL MICROSCOPY, IMAGE RECONSTRUCTION AND ISOSURFACE RENDERING: APPLICATION TO GLIAL CELLS IN MOUSE CENTRAL NERVOUS SYSTEM

Frank Morgan[1], Elisa Barbarese[2], John H. Carson[1] *

Departments of [1]Biochemistry and [2]Neurology
University of Connecticut Health Center
Farmington, CT 06030

(Received for publication December 20, 1991, and in revised form March 24, 1992)

Abstract

This paper describes a general method for visualizing individual cells in intact tissue in three dimensions. The method involves immunostaining intact tissue to label specific cells, "optical sectioning" the stained tissue by laser scanning confocal microscopy, computationally reconstructing a three dimensional image data set from the digitized confocal optical sections, delineating isosurfaces of specific intensity within the reconstructed image by a "marching cubes" algorithm to generate polygon meshes defining boundaries of cells, and displaying individual cells, identified as three dimensional objects enclosed by contiguous polygon meshes, using computer graphics techniques. Each of the components of this method has been described previously in conjunction with other applications. However the combination of these techniques to visualize a variety of different individual cell types in three dimensions in intact tissue represents a new approach.

To illustrate the application of this method, we have visualized three different glial cell types in mouse CNS tissue. Oligodendrocytes, specifically stained with antibody to myelin basic protein, were used as an example of cells labelled with an internal membrane antigen. Astrocytes, specifically stained with antibody to glial fibrillary acidic protein, were used as an example of cells labelled with a cytoplasmic antigen. Microglia, specifically stained with Mac.1 antibody, were used as an example of cells labelled with an external membrane antigen. The images that are generated contain remarkably detailed volumetric and textural information that is not obtainable by conventional imaging techniques.

Key Words: Oligodendrocyte, astrocyte, microglia, confocal microscopy, image reconstruction, three dimensional imaging, isosurface rendering, computer graphics, myelin basic protein, glial fibrillary acidic protein, Mac.1 antigen.

*Address for correspondence:
John H. Carson
Department of Biochemistry
University of Connecticut Health Center
Farmington, CT 06030

Phone No.: (203) 679-2130
Fax No.: (203) 679-3408

Introduction

Cells are three dimensional objects embedded in a three dimensional tissue environment. Conventional light and electron microscopy are imaging techniques optimized for resolution in the x and y axes with limited resolution in the z axis. This means that the three dimensional volume properties and surface texture characteristics of the cell are not imaged effectively by conventional microscopic techniques. Historically, microscopists have attempted to overcome this limitation in a variety of ways. One method involves examining the cell at different focal planes to estimate its three dimensional properties. This relies on the interpretive ability of the microscopist and does not yield an accurate representation of the relevant dimensions suitable for measurement. Another method involves physically sectioning the cell, imaging the individual sections in two dimensions and then reconstructing a three dimensional representation of the cell by superimposing the individual section images. This disrupts the tissue environment, introducing potential artifacts due to shearing, shrinkage or tearing during sectioning. Registration between adjacent sections is also a problem and this approach is limited in resolution by the thickness of the sections that can be cut. In this paper we describe a method that circumvents these problems by directly visualizing cells at high resolution in three dimensions in intact tissue.

In this method, the data are collected by "optically sectioning" the tissue using confocal microscopy, which avoids disruption of the tissue environment. A three dimensional image data set is reconstructed computationally from the optical sections without relying on the interpretive ability of the microscopist. Finally an informative three dimensional image of the cell is displayed using computer graphics techniques. This method generates striking images of individual cells with detailed information concerning volume properties and surface texture characteristics that is not obtainable by conventional imaging techniques.

There are four requirements for such a method. First, individual cells must be specifically labelled. Second, a series of high resolution scanned images must be collected at different focal planes from the intact tissue in a nondisruptive way. Third, a three dimensional image must be reconstructed computationally from the series of scanned images. Fourth, an informative three dimensional representation of the individual cell must be extracted from the total reconstructed image data and rendered in a way that reveals the volume properties and

surface texture characteristics of the cell. Recent technological developments in confocal microscopy and three dimensional computer graphics now make such a method feasible.

The principle of confocal microscopy has been recognized for many years (for review see Minsky, 1988). However, only recently have improvements in implementation (White *et al.*, 1987) and commercial production made this technology widely available. The confocal microscope rejects light emitted from above or below the focal plane, thereby improving the effective resolution of the microscope in the *z* axis. This provides the capability of optically sectioning a sample by collecting a series of scanned images at different focal planes. Such a series of optical sections represents a high resolution three dimensional image data set through the sample. Theoretical and practical aspects of confocal microscopy of biological specimens are discussed in detail in several recent books (see for example Pawley, 1990).

Image reconstruction from series of optical sections involves the assignment of spatial coordinates to each intensity value in the data set. In the case of confocal microscopic data, each optical section consists of a two dimensional array of digitized intensity values associated with specific *x*, *y* coordinates. Since the distance between consecutive optical sections is known, and since the optical sections are collected sequentially, and are in perfect register, a *z* coordinate can also be assigned to each data point based on the known distance between successive optical sections. Thus each data point can be assigned a specific *x*, *y* and *z* coordinate corresponding to a particular location in the original sample. This effectively reconstructs a three dimensional image from the optical section data set.

There are two general methods for rendering three dimensional images, both of which rely on advanced graphics computing techniques. The first method is called volume rendering. In this method each data point in the reconstructed image is represented as a cubic volume element or "voxel" carrying the intensity value associated with the original image data point. The voxels are stacked in order and then projected into a two dimensional picture. Using appropriate pseudocolor, transparency, lighting, contrast and animation techniques for depth cueing, this provides an informative three dimensional visualization method for certain types of data. It is particularly useful for visualizing diffuse distributions of components within cells. Its main advantage is that it displays all of the data. Its main disadvantage is that image quality may be degraded when viewed at close range because the voxel structure becomes noticeable.

The second method is called surface rendering (Cline *et al.*, 1988). In this method, the three dimensional array of data points is converted into voxels which are traversed using a "marching cubes" algorithm to generate meshed polygons which define isosurfaces of specific intensity within the original data set. The isosurfaces can then be displayed with appropriate lighting, Gouraud shading, perspective, Z-buffering and animation to generate an informative three dimensional image. This method is particularly useful for visualizing discrete surfaces in cells. Its main advantage is that it produces a sharp highly resolved image that can be examined at close range without degrading image quality. Its main disadvantage is that it requires *a priori* selection of a specific boundary intensity. A variety of more specialized methods for rendering three dimensional images from light or electron microscopic serial section data have also been described (Schormann and Jovin, 1990; Moss *et al.*, 1990; Montag *et al.*, 1990; Lockhausen *et al.*, 1990; Bron *et al.*, 1990).

In this paper, we describe the use of immunological staining, optical sectioning by confocal microscopy, computerized image reconstruction and surface rendering to visualize whole cells in three dimensions. To illustrate the method we have visualized the three major glial cell types in mouse CNS: oligodendrocytes, which produce myelin; astrocytes, which perform a variety of functions such as maintenance of ionic homeostasis (Newman, 1985), formation and maintenance of the blood-brain barrier (Senjo *et al.*, 1986), synthesis and secretion of growth factors (Lillien *et al.*, 1988) and lymphokines (Benveniste, 1988), guidance of neuronal migration and axonal outgrowth, and scavenging of neurotransmitters (Hertz, *et al.*, 1978); and microglia, whose function is phagocytosis. These cells were chosen because they pose a challenge to microscopic methods. They are interspersed randomly throughout the tissue without exhibiting characteristic layering or other defined structural organization. They have multiple long processes extending in many different directions in three dimensions. And they exhibit fine structural features that are at the limit of resolution of the light microscope.

The different glial cells express different unique antigens and thus can be specifically labelled with antibodies. Oligodendrocytes express myelin basic protein (MBP), which is a membrane protein found only in these cells and the myelin sheaths they produce. Astrocytes express a characteristic intermediate filament protein called glial fibrillary acidic protein (GFAP). This protein forms a pervasive cytoskeletal network in the cytoplasm of the cell. Microglia express Mac.1, which is a cell surface antigen unique to these cells in the CNS (Matsumoto *et al.*, 1985).

The three glial cell types also display quite distinct morphological features. Oligodendrocytes have a small, oval perikaryon with a smooth contour. They extend multiple thin, smooth processes, each of which flattens out and wraps around a segment of axon in a spiral fashion producing a myelin internode (reviewed in Penfield, 1932; Wood and Bunge, 1984; Sternberger *et al.*, 1978). Astrocytes assume a variety of different morphologies which is consistent with their plethora of functions (reviewed in Penfield, 1932). Generally, astrocytes are more asymmetric in shape than oligodendrocytes, with several long, branched processes which may terminate in end-feet abutting other cells, the pia mater, or blood vessels. Astrocytes contain fibrils (intermediate filaments) that most often are underlying the cell surface. Mature microglia are dendritic cells with processes that become thinner as they elongate from the cell body. The processes are wavy and covered with numerous thin, small spines. The cell body of the microglia appears "spongy" in certain preparations (Del Rio Hortega, 1932; Ling, 1981).

The images of oligodendrocytes, astrocytes and microglia obtained in this study by confocal microscopy, computerized image reconstruction and surface rendering are consistent with previous descriptions of these cells derived from conventional microscopic observations. In addition they reveal volume properties and surface texture characteristics that are not revealed by conventional imaging techniques. The techniques of confocal microscopy, computerized image reconstruction and surface rendering have been described previously in

conjunction with other applications. However, the combination of these techniques to analyze the three dimensional properties of glial cells in intact CNS tissue, as described here, represents a new approach to studying cellular morphology in intact tissue and the quality of the images that are generated illustrates the suitability of this approach.

Materials and Methods

Animals

Breeding pairs of C57BL/6J mice were originally purchased from Jackson Labs (Bar Harbor, ME) and were subsequently propagated by brother-sister mating. Mice were maintained in the Center for Laboratory Animal Care at UCHC. Animals were sacrificed by cervical dislocation after ether anesthesia according to the guidelines for the care of laboratory animals.

Tissue sections

One cerebral hemisphere was dissected out, embedded in agarose, and sectioned (200μm) with a tissue chopper. Fresh sections were processed immediately for immunocytochemistry with Mac.1 antibody. The other cerebral hemisphere and the optic nerves were fixed for 48 hours in 4% phosphate-buffered paraformaldehyde containing 5mM $MgCl_2$, pH 7.6. Sections (100 μm) were cut from the cerebral hemisphere with a vibratome and stored in 0.1M phosphate buffer (pH 7.6) until processing for immunocytochemistry. Optic nerves were stored in phosphate buffer, as described above, but were used whole for immunocytochemistry.

Immunocytochemistry for internal antigens

Vibratome sections (100 μm) were free-floated in 0.05M Tris-HCl pH 7.6 containing 5% normal goat serum (NGS) and permeated with detergent (0.1% NP-40) in 0.05M Tris-HCl pH 7.6 for one hour at room temperature. Sections were then rinsed with buffer (2 x 15 min) and incubated overnight at 4° C in a 1:100 dilution of rabbit anti-GFAP (Accurate), or in a 1:50 dilution of rabbit anti-MBP (Barbarese *et al.,* 1977) in detergent (0.1% NP-40) and serum (5% NGS)-containing buffer. Following buffer rinses (4 x 15 min) at room temperature, the sections were incubated overnight at 4° C with a 1:50 dilution of fluorescein conjugated goat anti-rabbit IgG (Organon-Cappel) in detergent and serum-containing buffer. Sections were rinsed again, mounted and coverslipped with 3% 1,4-diazabicyclo[2.2.2.]octane (DABCO) in glycerol.

Immunocytochemistry for surface antigens

The method is essentially that of Warrington and Pfeiffer (1990) with minor modifications. Fresh sections (200 μm) were incubated in Dulbecco's balanced salt solution supplemented with 6.5 mg/ml glucose, 0.3% bovine serum albumin (BSA), and 4.77 mg/ml HEPES (DGBH) for 3 hours at 4°. The sections were then transferred into the first antibody, Mac.1 (Boehringer-Mannheim) (1:40 in DGBH), and incubated overnight at 4°. The sections were rinsed (3 x 15 min) with DGBH, and fixed in 4% phosphate-buffered paraformaldehyde for 3 hours at 4°. The sections were rinsed in 1% BSA in 0.1M phosphate buffer, pH 7.6, and incubated in the same buffer containing fluorescein-conjugated goat anti-rat antibody (Organon-Cappel) (1:50), overnight at 4°. The sections were then rinsed with the BSA-containing buffer, and mounted as described above.

Confocal Microscopy

Confocal microscopy was performed with an MRC-600 system (Biorad) equipped with an argon ion laser and version 4.2 of the MRC software. The scan head is attached to an upright Zeiss Axioskop microscope equipped with several high numerical aperture objectives. Most of the images were collected using a Nikon 60X, 1.4 NA oil immersion objective. Unless otherwise indicated, optical sections were collected so that the pixel size was 0.15 μm x 0.15 μm, and the *z* axis interval was 0.5 μm. Images were collected at slow scan rate (4 sec/scan) with enhanced sensitivity, and were averaged over several scans to improve image quality.

Image reconstruction and rendering

Image reconstruction and rendering were performed with a Silicon Graphics IRIS 340 VGX graphics supercomputer equipped with 128 megabytes of memory and a variety of hard disc and optical disc storage devices. Image data were transferred by Ethernet from the microcomputer controlling the confocal microscope to the IRIS. The raw data were subjected to 4 cycles of two dimensional median smoothing to reduce noise in the individual optical sections. Appropriate *x*, *y* and *z* coordinates were assigned to each data point based on the image collection parameters, and the smoothed data were displayed as a three dimensional matrix of points. Boundaries delineating cell surfaces of interest were chosen empirically by rendering the matrix at a series of different boundary intensities and choosing the maximum value which left the outlines of the cell intact. The entire data set was traversed using a "marching cubes" algorithm (described in the Results section) to generate meshed polygons defining isosurfaces at the selected boundary intensity within the original data set. The polygons were grouped into contiguous meshes delineating discrete objects. The polygon mesh delineating the cell surface was then displayed with appropriate lighting, Gouraud shading, perspective and Z-buffering to generate a three dimensional image. Scale bars were embedded within the image to facilitate size estimation. Images were photographed directly from the monitor of the IRIS.

Results

In this section, we will describe in detail the steps in the procedure for three dimensional visualization of cells in intact tissue, using the oligodendrocyte in mouse optic nerve as an example of a cell stained with antibody to an internal membrane antigen, MBP. Then we will describe three dimensional visualization of astrocytes and microglial cells in mouse CNS tissues as examples of cells stained with antibody to a cytoplasmic antigen, GFAP, and an external membrane antigen, Mac. 1, respectively. Each example will illustrate different aspects of the visualization procedure.

Confocal optical sectioning through a mouse oligodendrocyte

Figure 1 shows a series of confocal optical sections through an oligodendrocyte in a mouse optic nerve that has been stained with antibody to MBP. Each section contains only a portion of the cell body or segments of myelin sheath produced by the cell. In some cases, the section passes longitudinally through the center of an axon revealing the unstained interior of the axon. Although MBP is predominantly a membrane protein, the interior of the oligodendrocyte cytoplasm is diffusely stained indicating that at least some MBP is present in the cytoplasm. The interior of the nucleus is not stained.

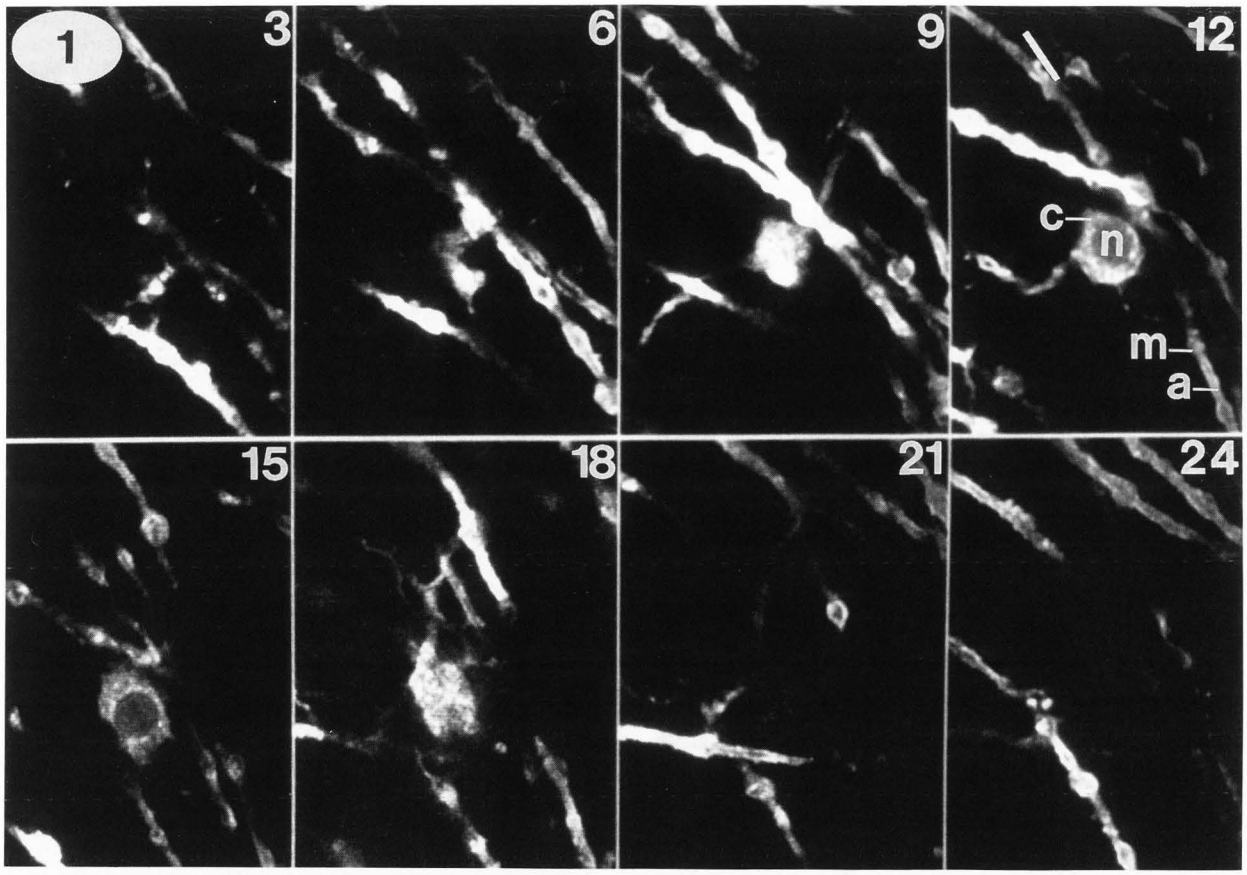
1
3
6
9
12
c
n
m
a
15
18
21
24

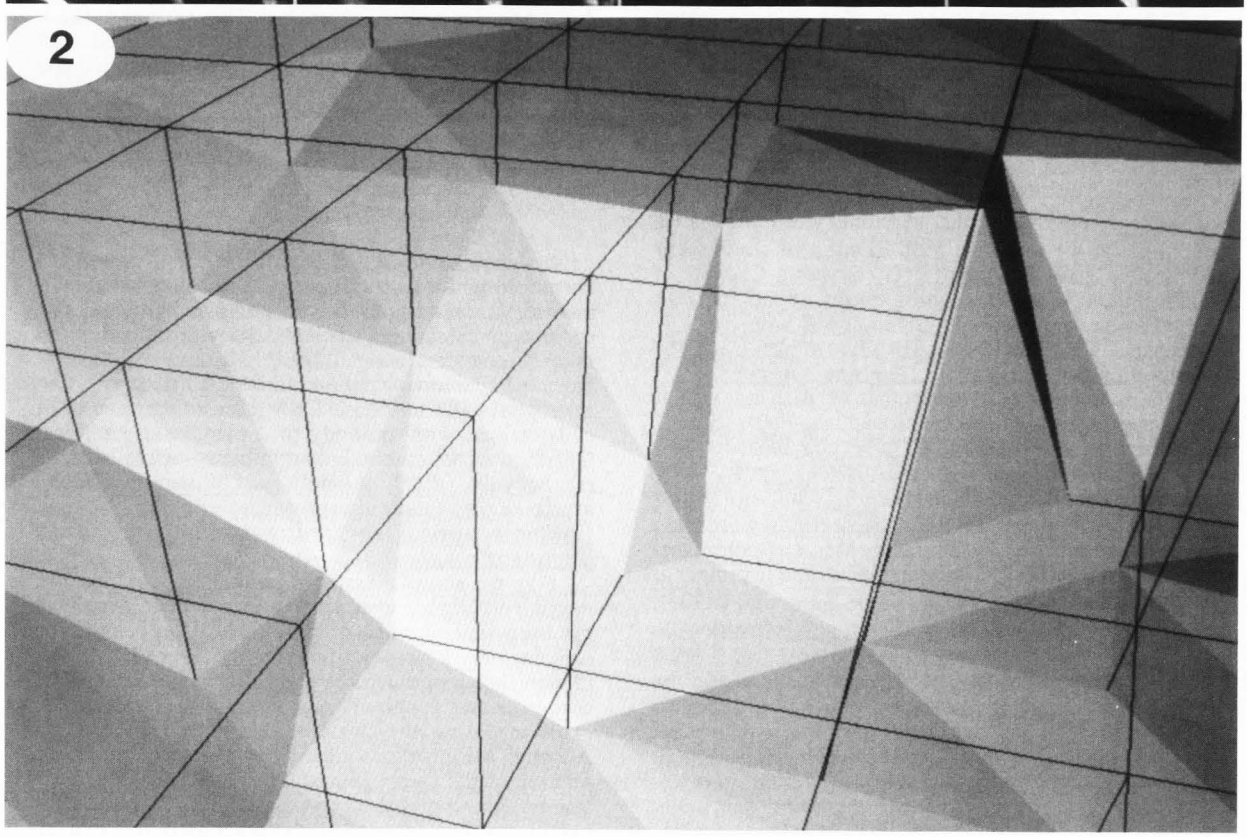
2

Figure 1. Confocal optical sections through a mouse oligodendrocyte labelled with antibody to MBP.

Mouse optic nerve was labelled with antibody to MBP as described in Materials and Methods. The intact nerve was examined by confocal laser scanning microscopy using a Nikon 60x, 1.4 NA oil immersion objective. A typical oligodendrocyte was identified and 30 optical sections (384 x 512 pixels at 0.5 µm intervals) were collected. Each frame was averaged over 5 scans to improve image quality. The gain and black levels were set manually to optimize the dynamic range in the image while ensuring that no region was completely black (intensity=0) or completely saturated (intensity=255). A representative selection, consisting of every third section, is displayed, from image 3 in the upper left corner through image 24 in the lower right. Symbols: a = axon, c= cell body, m = myelin, and n = nucleus.

Figure 2. Marching cubes isosurface extraction.

The data shown in figure 1 were computationally reconstructed into a three dimensional matrix of intensity values and analyzed by the "marching cubes" algorithm to define an isosurface, as described in Materials and Methods. A small subset of the data is shown. Voxels are outlined in black. The intersections of the black lines indicate the coordinates of intensity data points in the matrix which define the vertices of the voxels. The polygons intersecting each voxel are flat-shaded based on the angle between their normals and the incident light. Voxels not intersected by polygons are not shown.

Sternberger *et al.*, (1978), using immunostaining of thin sections, have also reported MBP staining in the cytoplasm of oligodendrocytes, particularly in immature cells. Taken together, these optical sections comprise a complete three dimensional data set describing the distribution of MBP in the oligodendrocyte.

Image reconstruction from confocal optical sections

Each of the optical sections in figure 1 consists of a two dimensional array of digitized intensity values. Each point in the array has specific *x* and *y* coordinates. Since the sections were collected consecutively at fixed intervals in the *z* axis, and since the sections are in perfect register, each point can also be assigned a specific *z* coordinate. Thus, the data can be reconstructed into a three dimensional matrix, as illustrated in figure 2, where each data point, indicated by the intersections of the black lines, consists of an intensity value associated with a specific *x*, *y* and *z* coordinate, corresponding to a particular three dimensional location in the original specimen.

The data were collected so that the point density was matched to the resolution of the confocal microscope. The resolution of a microscope is determined by the shape of the three dimensional point spread function which describes the way a point source of light is dispersed in three dimensions after it passes through the optical path of the microscope. In the case of the confocal microscope, the point spread function resembles an oblate spheroid whose long axis is aligned with the *z* axis of the microscope (White *et al.*, 1987, Shaw and Rawlins, 1991). This means that the resolution of the microscope is somewhat greater in the *x* and *y* axes than in the *z* axis. Accordingly, data were collected so that the distance between adjacent points in the *x* and *y* axes in each optical section approximates the width of the three dimensional point spread function, while the distance between adjacent optical sections in the *z* axis approximates the length of the three dimensional point spread function. This maximizes the information content of the data set while minimizing laser exposure of the sample.

Isosurface rendering of three dimensional images

If all the data points in the reconstructed three dimensional array are displayed simultaneously, the resulting image is difficult to interpret. We reasoned that a more informative image could be obtained if certain features of interest could be extracted from the data and displayed separately. One major feature of interest is the cell surface. If the preparation is labelled with an antibody to a plasma membrane component or to a component that fills the cytoplasm, then points outside the cell will have lower intensities and points inside the cell will have higher intensities. The cell membrane will be delineated by a boundary of specific intensity within the data set.

Surfaces are displayed by graphics computers as meshed arrays of polygons. Thus, in order to extract and display the cell surface from the three dimensional data set it is necessary to define a set of polygons that delineates a boundary surface of specific intensity within the data. This can be accomplished using the "marching cubes" algorithm described by Cline *et al.*, (1988) as a method for three dimensional reconstruction of tomograms. According to this algorithm, a three dimensional array of data points is converted into a set of polygons by subdividing the data set into voxels and sequentially examining each voxel.

A voxel is defined by eight vertices, four each from two adjacent optical sections. Each vertex can have one of two possible states, either inside or outside the feature of interest, depending on whether the intensity of the vertex point is above or below the specific boundary intensity. According to Polya's theorem, there are 15 topologically distinct configurations for the vertices of a cube where each vertex is in one of two possible states (Harary, 1969). Thus, each voxel in the data set can be indexed to one of 15 possible topological configurations.

The topological configurations of the vertices of each voxel determines whether or not a surface intersects that voxel, and if so, what shape the intersecting polygon assumes. For example, a voxel with one inside vertex and seven outside vertices will be intersected by a triangular polygon whose vertices are located on the three edges of the voxel originating at the single inside vertex. The pattern of polygons intersecting a particular voxel is termed the tesselation pattern. There is a different tesselation pattern corresponding to each of the 15 different topological configurations of vertices. Thus, the tesselation pattern for a particular voxel can be determined by reference to a look up table converting the topological configuration of vertices to the corresponding tesselation pattern.

While the tesselation pattern of a particular voxel is determined by the topological configuration of the vertices, the position(s) of the intersecting polygon(s) within the voxel is determined by the actual intensity values at the vertices. For example, if the intensity value at one corner of a voxel is just slightly above the boundary threshold and at an adjacent corner is far below the boundary threshold then the position of the intersecting polygon will be closer to the corner of the voxel whose intensity is nearest to the boundary threshold intensity. The actual position of the intersecting polygon is determined by finding the boundary intensity

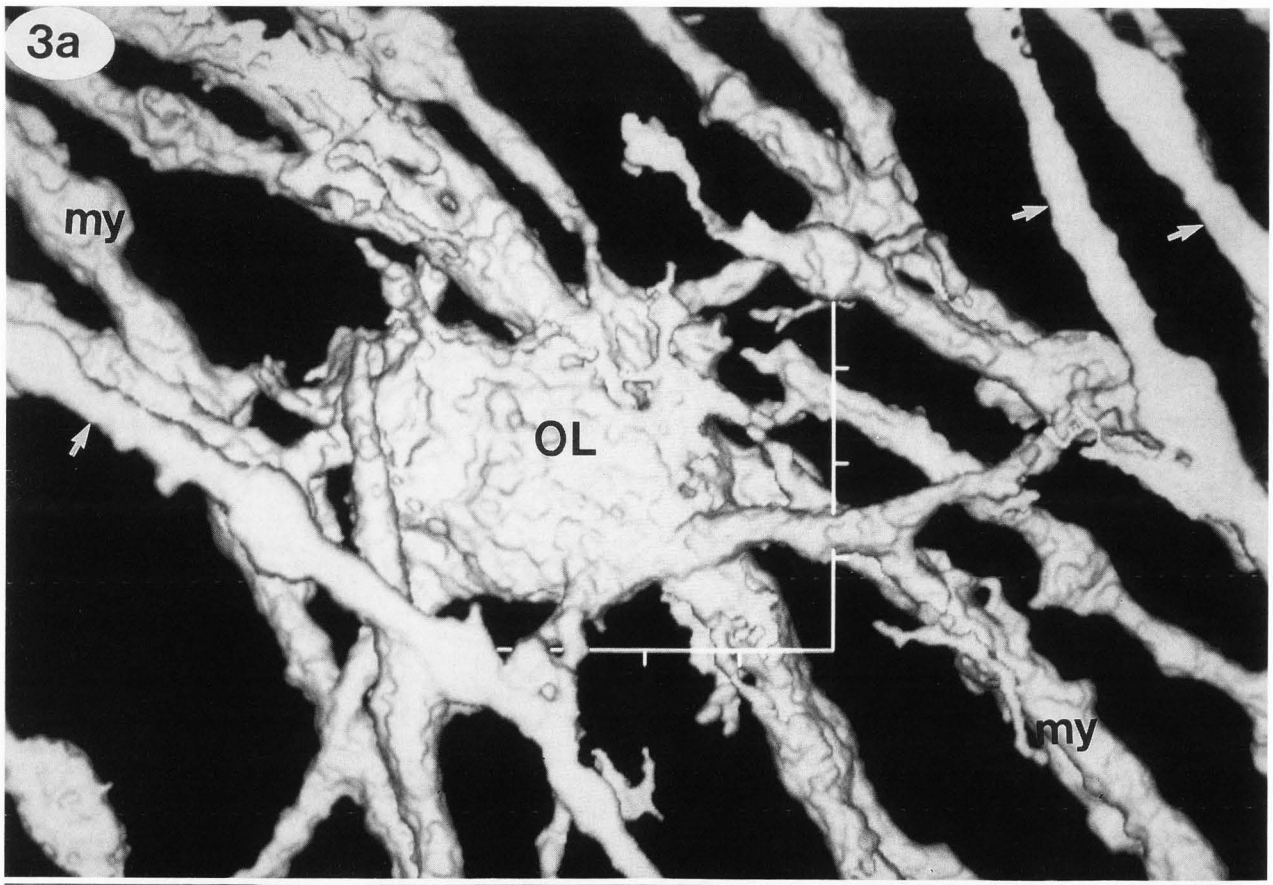
3a
my
OL
my

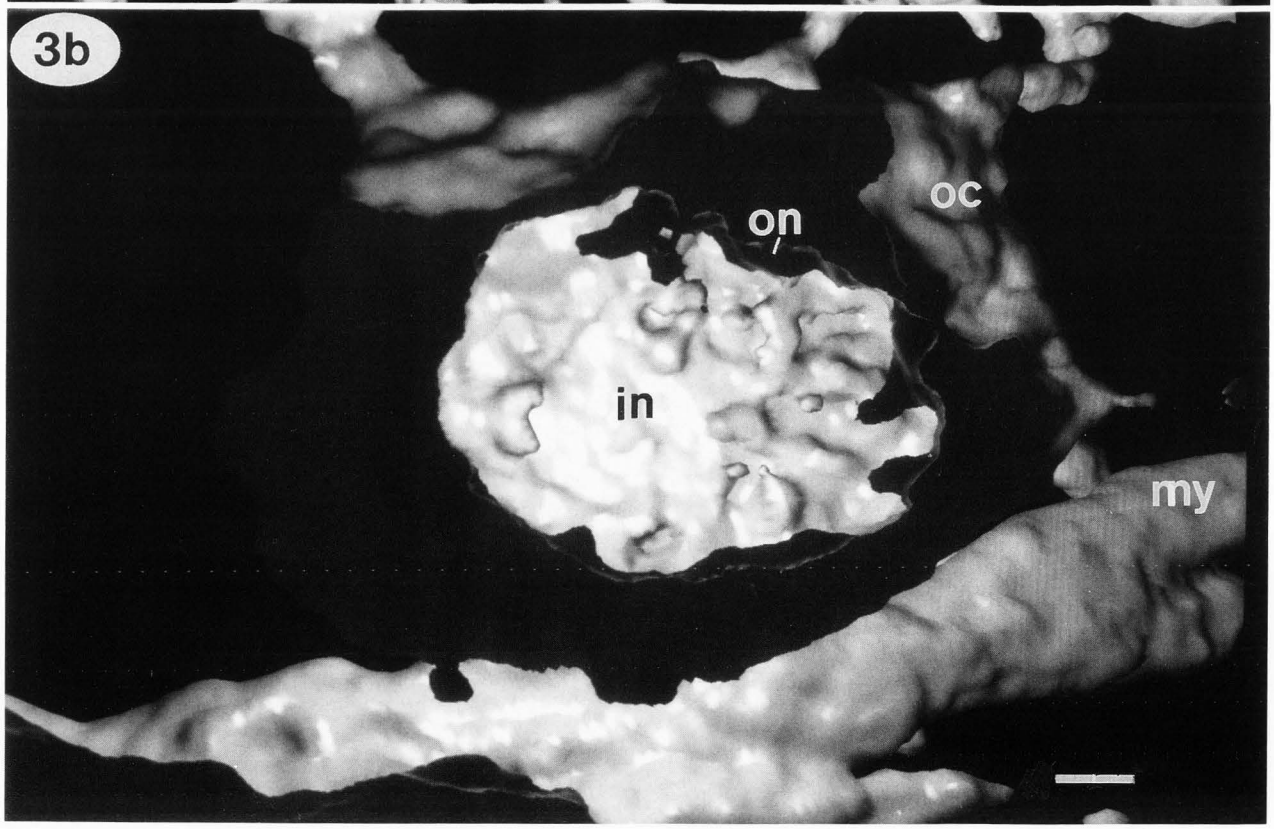
3b
on
oc
in
my

Figure 3. Isosurface rendering of an oligodendrocyte labelled with antibody to MBP.
The data from figure 1 were reconstructed and subjected to isosurface extraction, object detection, and rendering as described in Figure 2 and in the text.

Panel a: The isosurface value was set at 50 to delineate the plasma membrane and myelin sheaths. The L shaped scale bar embedded in the image has tick marks at 5 μm intervals. The arrows point to regions where features of the cell extended beyond the limits of the data set and were truncated when the data were collected. Symbols: my = myelin, and OL = oligodendrocyte. The image consists of a continuous mesh of 745,622 polygons.

Panel b: Several sections have been removed to reveal the interior of the oligodendrocyte perikaryon shown in Panel a. The isosurface value was set at 115 to delineate the boundary between the unstained nucleus and the stained cytoplasm. The shininess and specular reflectance of the polygon mesh were increased and the light source was moved closer to the object in order to enhance the differentiation of nuclear envelope versus plasma membrane. The scale bar represents 2μm. Symbols: in = inside nuclear membrane, on = outside nuclear membrane, oc = outside cell membrane, my = myelin membrane.

---

within a linear interpolation between the intensity values at the two corners of the voxel.

In summary, extracting an isosurface from a three dimensional array of intensity values involves the following steps: 1) subdividing the data into voxels; 2) classifying the eight vertices of each voxel by comparing their intensity values to a specific boundary intensity; 3) indexing each voxel on the basis of the topological configuration of its vertices; 4) determining the tesselation pattern of each voxel from the index of its topological configuration of vertices; 5) positioning the intersecting polygon(s) within each voxel based on the intensity values at its vertices; 6) traversing the entire data set by this "marching cubes" algorithm. This procedure will generate a meshed set of polygons that delineates a three dimensional isosurface contained within the original three dimensional array of data.

An example of the results obtained by applying this procedure to a small subset of the data in figure 1 is shown in figure 2. The voxels are outlined in black and the meshed polygons are shown in various shades of grey. It is apparent that the polygons delineate a surface. The texture of the surface appears facetted because the individual polygons are flat shaded with a single normal value associated with each polygon. The angle between the normal and the incident light determines the brightness or intensity of the entire polygon. However, most biological surfaces, such as the cell surface, are smoothly continuous. To make the polygonal surface mesh appear smoother and more continuous we have employed a technique called Gouraud shading (Gouraud, 1971). In this procedure, the normals for all of the polygons surrounding each vertex in the mesh are averaged to generate a resultant normal for that vertex which presumably approximates the true normal for the surface at that point. The intensity at each vertex is calculated based on the angle between the incident light and the resultant normal at that vertex. The intensity in the areas between the vertices is calculated by bilinear interpolation from the intensities at the vertices. This generates smooth continuous intensity variations over the polygon mesh, more accurately representing the actual cell surface. Examples of Gouraud shading are shown in Figures 3, 4 and 5.

Object detection in isosurface images

Often a three dimensional data set will contain more than one cell or fragments of extraneous cells, which complicate the rendered isosurface image of the cell of interest. In order to eliminate extraneous surfaces from the image, it is necessary to isolate the surface of the cell of interest as a separate object. The polygons defining a discrete object form a continuous mesh, in which at least one vertex of each polygon is shared by another polygon in the same mesh. Thus, the polygon list for a particular three dimensional image can be subdivided into groups of polygons. All the members of one group share at least one vertex with at least one other member of the same group. This generates a list of separate objects in the three dimensional reconstructed image. The object corresponding to the cell of interest can then be isolated and displayed separately from extraneous cells and cell fragments. This procedure successfully separates the surface of the cell of interest from extraneous surfaces provided that none of the extraneous surfaces intersects any of the voxels delineating the cell of interest. In other words the surface of the cell of interest must be resolved from extraneous surfaces in the original data set.

Isosurface rendering of an oligodendrocyte stained with antibody to MBP

An isosurface image of an oligodendrocyte, reconstructed from the confocal optical sections in figure 1, is shown in figure 3A. An L-shaped scale bar is embedded in the image. Conventional scale bars can be misleading in this type of image because of perspective effects. The oligodendrocyte cell body is visible in the center of the image. The surface texture of the cell body is quite complex with many dimples and bumps. Thin processes emanate from the perikaryon and terminate in thicker myelin sheaths which traverse the image. This particular cell has elaborated approximately 20 myelin internodes. Some of the myelin sheaths, which extend outside of the original data set, appear in longitudinal section, and are rendered with flat surfaces devoid of texture. The myelin sheaths are made up of many wrappings of membrane around axons (which are unstained in this preparation). The outer wrapping of the myelin sheath often contains a pocket of cytoplasm (called the outer mesaxon) which causes a longitudinal bulge in the sheath. Outer mesaxon bulges can be discerned along several of the myelin internodes. The dimensions of the oligodendrocyte cell body (10-20 μm in diameter), processes (1-12 μm in length) and myelin sheaths (2-3 μm in diameter) in the reconstructed image are comparable to the dimensions for this type of cell determined by conventional light and electron microscopy (Bunge, 1968; Wood and Bunge, 1984).

Computational dissection to reveal hidden surfaces

The marching cubes algorithm will define a surface intersecting any voxel which has at least one vertex above and one vertex below the specified boundary intensity. In a preparation such as the oligodendrocyte shown in figure 3A, which is stained with antibody to an antigen (MBP) that is present both in the plasma membrane as well as in the cytoplasm, isosurfaces will be defined at the external and internal surfaces of the plasma membrane since these represent interfaces between the outside of the cell and the membrane and the inside of the cell and the membrane, respectively. In addition, isosurfaces will be defined at any internal boundaries between antigen-containing and antigen-free compartments. Since MBP is

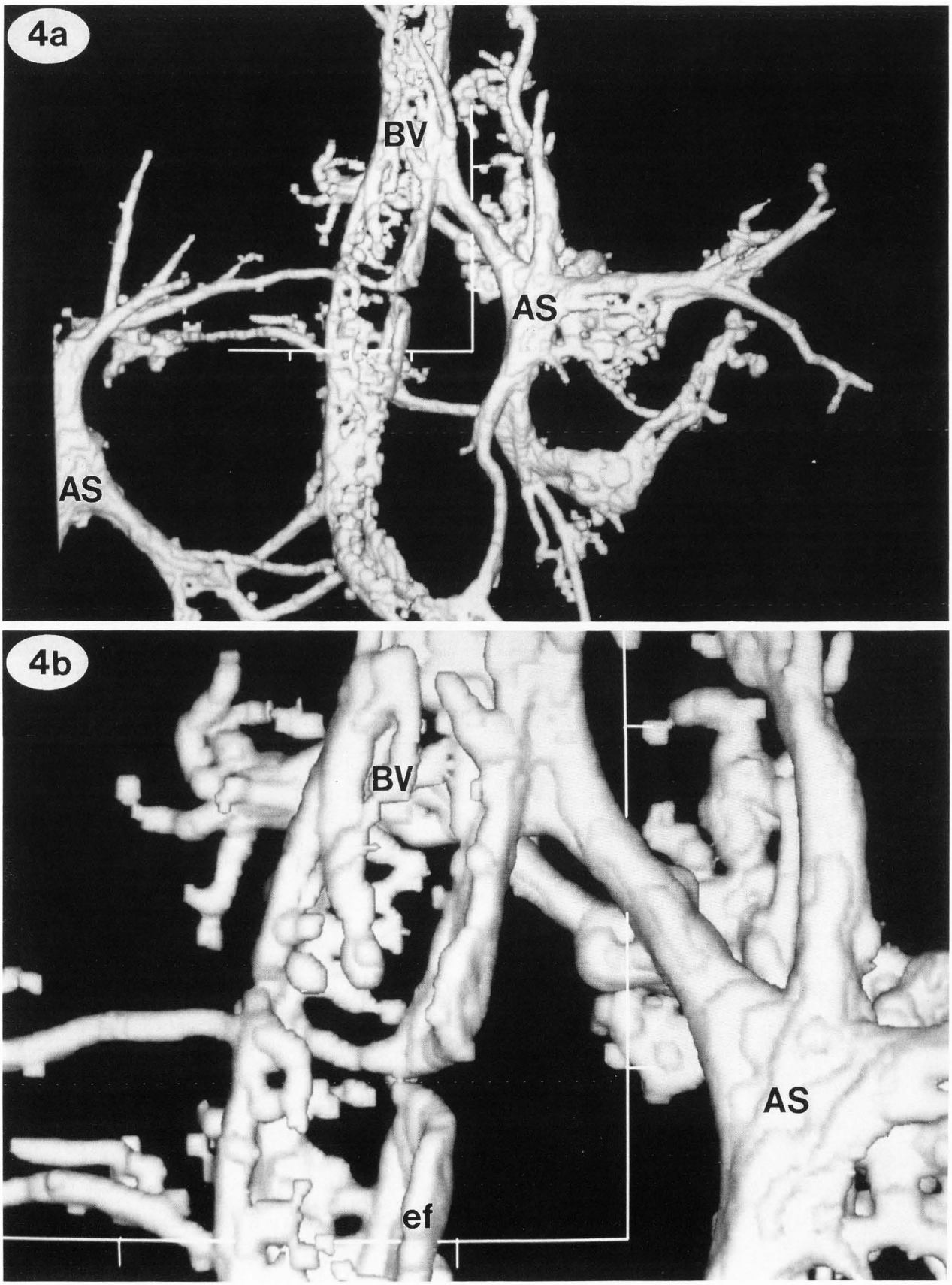
4a
BV
AS
AS
4b
BV
AS
ef

Figure 4. Isosurface rendering of astrocytes labelled with antibody to GFAP.

Confocal optical section data from a vibratome section of mouse cerebral hemisphere labelled with antibody to GFAP were reconstructed and subjected to isosurface extraction, object detection and rendering as described in the text. The isosurface value was 30 to delineate the boundary between the GFAP-filled cytoplasm of the cell and the exterior. The L shaped scale bar embedded in the image has tick marks at 5 μm intervals. Symbols: AS = astrocyte, and BV = blood vessel, and ef = endfeet.

Panel a: Portions of two perivascular astrocytes with endfeet surrounding a blood vessel. The image consists of a continuous mesh of 337,150 polygons.

Panel b: A subvolume of the image shown in Panel a viewed from a point closer to the object. The scale bar is in the same position relative to the object in Panel a and Panel b.

---

found in the cytoplasm but not in the nucleus of the oligodendrocyte (see Figure 1) there is an intensity boundary between the nucleus and cytoplasm. This boundary delineates the nuclear envelope and will be defined as an isosurface by the "marching cubes" algorithm. In Figure 3A the nuclear envelope surface is obscured by the overlying plasma membrane isosurface because the image is rendered with Z-buffering or hidden line removal. This enhances the three dimensional appearance of the cell by providing important depth cues. However, some surfaces of the cell are hidden or obscured by surfaces closer to point of observation. This includes the external surface of the cell facing away from the point of observation as well as internal surfaces, such as the nuclear envelope, within the cell. The cell surfaces which are obscured can be visualized by either computationally dissecting away the overlying surfaces or by translating the point of observation within the data set.

In order to remove the overlying plasma membrane isosurface obscuring the nuclear envelope isosurface in Figure 3A, the data were dissected so that the top half of the oligodendrocyte cell body, including the top half of the nucleus was eliminated. As shown in Figure 3B, this reveals the underlying isosurface corresponding to the outer and inner surface of the nuclear envelope. The surface of the inner aspect of the nuclear envelope is quite convoluted with numerous bumps and pits, some of which may correspond to nuclear pores. This illustrates one of the important advantages of surface rendering, which is that the image can be explored in three dimensions either by computationally dissecting away obscuring surfaces (as shown in Figure 3B), or by translating the point of observation within the volume of the data set (not shown).

Three dimensional visualization of astrocytes

In this example, GFAP staining is used to identify astrocytes in mouse CNS tissue. Isosurface rendering of the GFAP-filled space is used to visualize the immuno-positive cells in three dimensions. The process of isosurface extraction with GFAP-stained tissue is basically the same as with MBP-stained tissue. However, in the case of MBP-stained tissue, the plasma membrane and myelin sheath are stained preferentially, so the isosurface that is defined delineates the cell surface. In the case of GFAP-stained tissue, the membrane is not stained, so the isosurface that is defined delineates the boundary between the unstained exterior of the cell and the stained interior of the cell. This provides an approximation of the surface of the cell. However, if GFAP does not fill the cell completely, the isosurface will not coincide exactly with the cell surface. Therefore, the surface texture of the GFAP-filled space may not reflect the actual texture of the astrocyte cell membrane. Nevertheless, since GFAP is the best available cell-specific marker for astrocytes, we have rendered GFAP-stained astrocytes using the marching cubes isosurface algorithm, to illustrate the application of this technique to cytoplasmically stained cells.

Figures 4A and 4B show the three dimensional isosurface of a GFAP-labelled preparation from mouse brain. There are two astrocytes in this image. The perikaryon of the first cell is on the right. The perikaryon of the second cell is partially cut off at the left of the image. Both cells extend several processes towards a blood vessel (not stained) which traverses the image vertically from top to bottom. Astrocytic processes from both cells terminate in perivascular end-feet which embrace the blood vessel, interdigitating in some areas. The GFAP-positive surfaces of the astrocytes in figure 4 appear smoother than the oligodendrocyte surface in figure 3. The dimensions of the astrocyte cell body (diameter 10 μm) and perivascular end feet (diameter 1-2 μm) in the reconstructed image are comparable to the dimensions for this type of cell determined by conventional light and electron microscopy.

Three dimensional visualization of Mac.1-stained microglia

Figure 5 shows the three dimensional isosurface of a Mac.1-stained dendritic microglial cell from mouse cerebral hemisphere. The cell has several short thick processes, as well as some thinner ones. The surface texture of the microglial cell is much more convoluted than either the oligodendrocyte (Figure 3) or the astrocyte (Figure 4). The surface of the perikaryon is covered with a multitude of fingerlike projections. The processes are also covered with numerous stubby fingerlike projections many of which terminate in bulbs. These projections are generally less than 1 μm in diameter, which means that each projection is defined by polygons extracted from a small number of adjacent voxels in the original data set and thus, is at the limit of resolution of this visualization technique. The dimensions of the microglial cell body (diameter 15 μm) and processes (2-3μm in diameter, up to 40 μm in length) in the reconstructed image are comparable to the dimensions for this type of cell determined by conventional light and electron microscopy (Perry *et al.*, 1985).

Discussion

We have described a general method for three dimensional visualization of cells in intact tissue. The method combines confocal laser scanning microscopy with computer-assisted image reconstruction and isosurface rendering to generate images containing detailed information about the spatial properties and surface texture of the cell. The method is rapid and convenient and avoids the shearing and cutting distortions associated with physical sectioning of tissue.

To illustrate the application of the method we have visualized three different types of glial cells, oligodendrocytes, astrocytes and microglia, in mouse CNS tissue *in situ*. The three dimensional properties of the three cell types revealed by this visualization method are consistent with previous notions of cell shape and size based on conventional light and electron microscopic observations. The image of an oligodendrocyte in intact tissue shown in figure 3 is remarkably similar to published diagrammatic representations of the

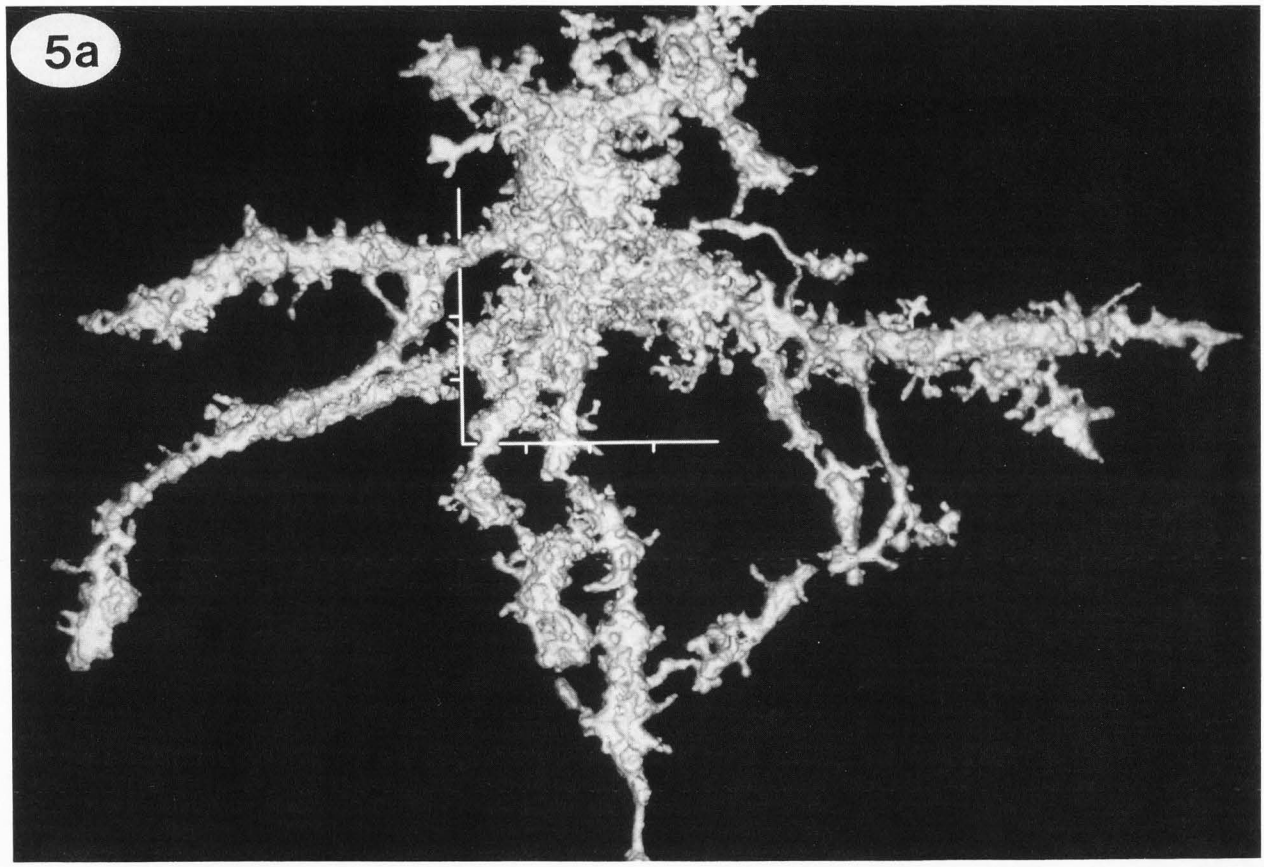
5a

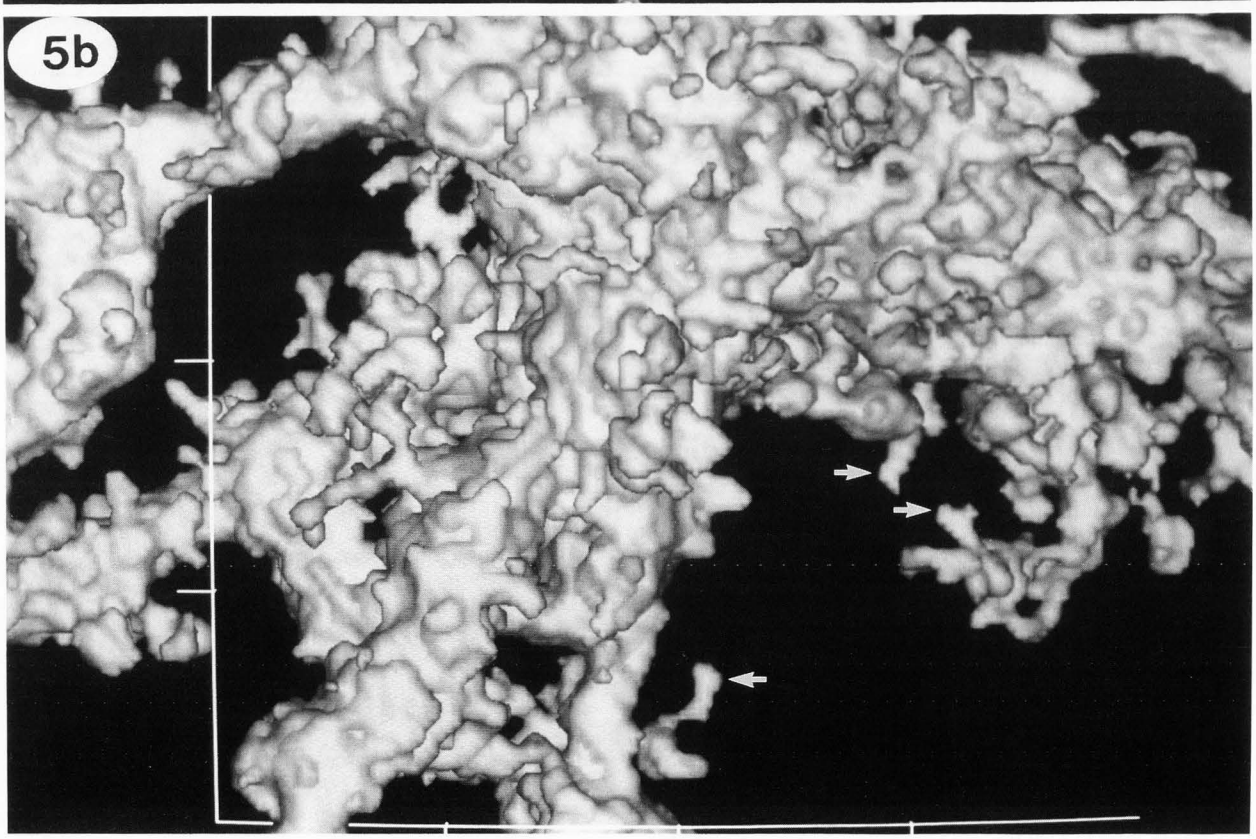
5b

Figure 5. Isosurface rendering of a microglial cell labelled with Mac.1 antibody.

Confocal optical section data from a fresh section of mouse cerebral hemisphere labelled with Mac.1 antibody were reconstructed and subjected to isosurface extraction, object detection and rendering as described in the text. The isosurface value was 30 to delineate the plasma membrane of the cell. The L shaped scale bar embedded in the image has tick marks at 5 μm intervals.

Panel a: A dendritic microglial cell. The image consists of a continuous mesh of 571,108 polygons.

Panel b: A subvolume of the image shown in Panel a. Arrows indicate structures that are at the limit of resolution. The scale bar is in the same position relative to the object in Panels a and b.

---

oligodendrocyte. The astrocytes shown in figure 4 are probably involved in the blood-brain barrier function having endfeet that appear to enmesh a blood vessel. The lacy network of perivascular endfeet revealed in the image is more complex than previously illustrated, but is consistent with narrative descriptions of these cells (Penfield, 1932). Finally, the features of the mature microglia shown in figure 5 correspond closely to those of the dendritic cells reported in classical light microscopy studies (Del Rio Hortega, 1932). Overall, the images generated by the visualization method described here are remarkably consistent with descriptions based on extrapolation from conventional sectioning and imaging techniques. This congruence of our results with results obtained by conventional imaging techniques validates the method of three dimensional visualization. We have also visualized fluorescent beads of various sizes using this method and the resultant images (not shown) provide further evidence that this is a faithful method for three dimensional visualization.

In addition to providing accurate visualization of the three dimensional space-filling or volumetric properties of the different cell types, the method also provides direct visualization of the surface texture of the cell. Since surface texture is not directly visualized, except in cross section, by conventional microscopy, there is no way to independently validate this aspect of the imaging method. However, the fact that the three physiologically different cell types display quite distinct surface textures argues that the textural details revealed by this visualization technique are physiological relevant and not artifact generated by the rendering procedure. In this regard, it is not clear to what extent the extreme complexity of the surface texture of the microglial cell with numerous stubby processes, and to a lesser extent the surface texture of the oligodendrocyte, with many ridges, bumps and dimples, faithfully reflect the surface texture of these cells *in vivo*, and to what extent some aspects of the surface texture may have formed during the fixation procedure. Every effort was taken to maintain isoosmolality during sample preparation. However if cell swelling or shrinkage or other physiological perturbations occurred this could be reflected in changes in the surface texture of the cell. Potential preparation artifacts notwithstanding, the surface textural details revealed by this visualization technique do appear to reflect physiological and functional differences between the different glial cell types in mouse CNS.

The isosurface rendering technique that we have described is particularly suitable for preparations that contain well defined surfaces or compartments with uniform fluorescent intensity. This creates clear cut boundaries at specific intensities which can be delineated by polygon meshes using the "marching cubes" algorithm. In general, we have found that preparations labelled with antibodies to cell membrane antigens or uniformly distributed cytoplasmic antigens can be informatively visualized in this way. Preparations containing patchy or non-uniform labelling or with gradients of antigen concentration throughout the volume are better visualized using volume rendering.

The resolution of the isosurface visualization method we have described is limited by the resolution of the confocal microscope. Under ideal conditions this is 0.1 - 0.2 μm in the x and y axes, and 0.5 - 1.0 μm in the z axis. Data are usually collected such that the distance between data points approximates the resolution limits in the x, y and z axes. It is possible to collect data at smaller intervals, but such "oversampling" aggravates the problem of photobleaching and photodamage, without significantly improving the resolution of the final image.

The dimensions of the voxel used in the "marching cubes" algorithm are determined by the intervals between data points (usually 0.1 - 0.2 μm in the x and y axes and 0.5 - 1.0 μm in the z axis). This means that if two surfaces are separated by less than these distances, they will impinge on the same voxel and will be fused together by the isosurface extraction algorithm. In other words, they will not be resolved. An example of this is seen in figure 4A, where the two astrocytes appear as one object because of their close apposition in the region of interdigitation of perivascular endfeet around the blood vessel. Nevertheless, this method provides significantly enhanced spatial resolution compared to conventional light microscopy, particularly in the z axis, and is capable of resolving fine details of surface texture that cannot be visualized by other techniques.

One potential application of the isosurface visualization technique not illustrated in this paper is surface area and volume determinations. The polygon mesh delineating a cell surface consists of a list of triangles. The area of each triangle is easily calculated from the coordinates of its vertices. The sum of the areas of the triangles making up the polygon mesh provides a measure of the surface area of the cell. Similarly, the number of voxels enclosed by the polygon mesh (with all vertices greater than, or equal to, the boundary intensity) can be determined. Since the volume of each voxel is known from the data collection parameters, the total enclosed volume can be calculated. With appropriate corrections for voxels intersected by the isosurface this provides a measure of the cell volume.

Acknowledgements

We would like to thank Dr. Kent Morest and Dr. Ann Cowan for reading the manuscript and providing valuable suggestions. This work was supported by NIH research grants to JHC (no. NS15190) and to EB (no. NS19943), an NIH Shared Instrumentation grant (no. RR03976), a State of Connecticut DHE Elias Howe grant and a University of Connecticut Health Center RAC equipment grant.

References

Barbarese E, Braun PE, Carson JH (1977) Identification of prelarge and presmall basic proteins in mouse myelin and their structural relationship to large and small basic proteins. Proc. Natl. Acad. Sci. USA 74, 3360-3364.

Benveniste EN (1988) Lymphokines and monokines in the neuroendocrine system. Prog. Allergy 43, 84-120.

Bron C, Gremillet P, Launay D, Jourlin M, Gautschi HP, Bachi T, Schupbach J (1990) Three dimensional electron microscopy of entire cells. J. Microscopy 157, 115-126.

Bunge RP (1968) Glial cells and the central myelin sheath. Physiol. Rev. 48, 197-251.

Cline HE, Lorensen WE, Ludke S, Crawford CR, Teeter BC (1988) Two algorithms for the three-dimensional reconstruction of tomograms. Med. Phys. 15, 320-327.

Del-Rio-Hortega P (1932) Microglia. In Cytology and cellular pathology of the nervous system. Vol. 2, ed. Wilder Penfield, Paul B. Hoeber Inc. New York, 483-534.

Gouraud H (1971) Illumination for computer generated pictures. Comm ACM 18, 311-317.

Harary F (1969) Graph Theory, Addison-Wesley, Reading, MA, 180.

Hertz L, Bock E, Schousboe A (1978) GFA content, glutamate uptake and activity of glutamate metabolizing enzymes in differentiating mouse astrocytes in primary cultures. Dev. Neurosci. 1, 226-238.

Lillien LE, Sendtner M, Rohrer H, Hughes SM, Raff MC (1988) Type-2 astrocyte development in rat brain cultures is initiated by a CNTF-like protein produced by Type-1 astrocytes. Neuron 1, 485-494.

Ling E-A (1981) The origin and nature of microglia. Adv. Cell. Neurobiol. 2, 33-82.

Lockhausen J, Kristen U, Menhardt W, Dallas WJ (1990) Three dimensional reconstruction of a plant dictyosome from series of ultrathin sections using computer image processing. J. Microscopy 158, 197-206.

Matsumoto Y, Watabe K, Ikuta F (1985) Immunohistochemical study on neuroglia identified by the monoclonal antibody against a macrophage differentiation antigen (Mac-1). J. Neuroimmunol. 9, 379-389.

Minsky M (1988) Memoir on inventing the confocal scanning microscope. Scanning 10, 128-138.

Montag M, Spring H, Trendelenburg MF, Kriete A. (1990) Methodological aspects of 3-D reconstruction of chromatin architecture in mouse trophoblast giant nuclei. J. Microscopy 158, 225-233.

Moss VA, McEwan Jenkinson D, Elder HY (1990) Automated image segmentation and serial section reconstruction in microscopy. J. Microscopy 158, 187-196.

Newman EA (1985) Regulation of potassium levels by glial cells in the retina. Trends in Neurosci. 8, 156-159.

Pawley JB (1990) Handbook of biological confocal microscopy. 1-214. ed. JB Pawley, Plenum Press, NY.

Penfield W (1932) Neuroglia: Normal and pathological. In Cytology and cellular pathology of the nervous system. Vol. 2, ed. Wilder Penfield, Paul B. Hoeber Inc. New York. 423-479.

Perry VH, Hume DA, Gordon S (1985) Immunohistochemical localization of macrophages and microglia in the adult and developing mouse brain. Neuroscience 15, 313-326.

Schormann T, Jovin TM (1990) Optical sectioning with a fluorescence confocal SLM: procedures for determination of the 2-D modulation transfer function and for 3-D reconstruction by tessellation. J. Microscopy 158, 153-164.

Senjo M, Ishibashi T, Terashima T, Inoue Y (1986) Correlation between astrogliogenesis and blood-brain barrier formation: Immunocytochemical demonstration by using astroglia-specific enzyme glutathione-S-transferase. Neurosci. Letters 66, 39-42.

Shaw PS, Rawlins DJ (1991) The point spread function of a confocal microscope: its measurement and use in deconvolution of 3D data. J. Microscopy 163, 151-165.

Sternberger NH, Itoyama Y, Kies MW, deF Webster H (1978) Myelin basic protein demonstrated immunocytochemically in oligodendroglia prior to myelin sheath formation. Proc. Natl. Acad. Sci. USA 75, 2521-2524.

Warrington AE, Pfeiffer SE (1990) Staining for myelin antigens in tissue slices. Trans. Am. Soc. Neurochem. 21, 243.

White JG, Amos WB Fordham M (1987) An evaluation of confocal versus conventional imaging of biological structures by fluorescent light microscopy. J. Cell Biol. 105, 41-48.

Wood P, Bunge RP (1984) The biology of the oligodendrocyte. In Oligodendroglia, Advances in Neurochemistry, Vol. 5, ed. WT Norton, Plenum Publishing Corp., New York. 1-46.

Discussion with Reviewers

B.R. Masters: Since the x=y but z-axis resolution is about 1/6 x-y resolution how does the 3-D volume rendering take this into account?

Authors: The data were collected so that the distance between adjacent points in the x-y plane (0.15 μm) approximates the limit of resolution in this plane and the distance between adjacent serial sections (0.5 μm) is slightly less than the limit of resolution in the z axis. Thus, the unit voxel defined by corresponding points in adjacent serial sections is not actually a cube but rather a parallelepiped with x and y dimensions equal to 0.15 μm and z dimensions equal to 0.5 μm. This does not affect the tessellation pattern for each voxel which depends only on the intensity values at each of the vertices. However the polygons that are calculated to intersect each voxel will tend to be slightly elongated in the z axis, reflecting the elongated z-axis dimensions of the voxel.

It is possible to generate cubic voxels by calculating a bilinear interpolation between the intensity values at corresponding positions in adjacent serial sections and inserting an appropriate number of calculated sections based on this interpolation. This procedure results in more symmetrical polygons which may produce a slightly more pleasing image. However this creates an impression of better resolution in the z axis than is actually achieved in the data, and for this reason we have avoided interpolating calculated sections. It could be argued that implementation of Gouraud shading of the polygons creates a similar effect.

We have examined the effect of the resolution differential between the x-y plane and the z axis on our rendering procedure by imaging fluorescent beads which are presumably perfectly spherical. The resulting images (data not shown) appear as smooth spheres with very little discernible surface texture except for some slight roughness on the top and bottom surfaces. This presumably reflects image noise at the boundary between the inside and outside of the bead which is detected in the x-y plane but which is averaged out between adjacent serial sections in the z axis.

S. Tai: Does the radius of incident light, e.g. fluorescent exposure, have to be considered while describing the surface texture characteristics?
Authors: The incident light in a confocal microscope is a scanned laser beam which is focused through the microscope objective. Therefore, the radius of the focused spot on the sample is dependent on the optical properties of the objective. Using photobleaching of a fixed fluorescent sample with a stationary centered beam focused through a 60X, 1.4 N.A. objective we have shown that the area bleached by the laser is a Gaussian spot with a radius of approximately 0.5 μm in the focal plane (data not shown). The radius of the beam is slightly greater above or below the focal plane or when the beam is scanned off-axis. Fluorescent light emitted from the sample is collected from a much smaller spot (with a radius of approximately 0.15 μm in most of our experiments) because the aperture in front of the photomultiplier rejects light emitted from outside this area resulting in a gain in the effective resolution of the system. Increasing the size of the aperture allows light to be collected from a larger area with a concomitant loss in resolution. Collecting light from a larger area will tend to average out local variations in intensity and thus may obscure some textural detail. However image noise also contributes to local intensity variations which are difficult to distinguish from actual variations. For this reason textural details that are delineated by small numbers of polygons should be interpreted with caution.

S. Tai: Is it possible to detect two different cell types in the same tissue using antibodies with different specificities and fluorophores with different wavelengths?
Authors: The MRC-600 confocal laser scanning system is equipped with an Argon ion laser light source which can be used to excite fluorophores at either 488 nm or 514 nm. Using appropriate combinations of filters and a second photomultiplier, it is possible to excite the sample at a single wavelength and simultaneously collect light emitted from two different fluorophores at two different wavelengths. Thus it is possible to simultaneously collect three dimensional image data on two different cell types in the same tissue. If the resulting isosurfaces are displayed in contrasting pseudocolor, the morphological relationships between the two cells can be visualized in exquisite detail (data not shown).